Mathematical Modelling and Numerical Analysis Will be set by the publisher
Modélisation Mathématique et Analyse Numérique

COMPARISON OF VLASOV SOLVERS FOR SPACECRAFT CHARGING SIMULATION

N. Vauchelet[1, 2], J.-P. Dudon[3], Ch. Besse[1, 4] and Th. Goudon[1,4]

Abstract. The modeling and the numerical resolution of the electrical charging of a spacecraft in interaction with the Earth magnetosphere is considered. It involves the Vlasov–Poisson system, endowed with non standard boundary conditions. We discuss the pros and cons of several numerical methods for solving this system, using as benchmark a simple 1D model which exhibits the main difficulties of the original models.

Résumé. Nous étudions la description mathématique de phénomènes de charge électrique auxquels sont soumis les satelittes interagissant avec la magnétosphère terrestre. Nous envisageons la résolution numérique de ces modèles qui prennent la forme de systèmes de Vlasov-Poisson mais avec des conditions aux bords inhabituelles. Nous discutons les avantages et inconvénients de diverses méthodes numériques en utilisant comme cas test un modèle 1D simplifié qui contient néanmoins les difficultés principales du modèle original.

1991 Mathematics Subject Classification. 82D10,65M25,76X05, 78A35.

.

Introduction

There is a growing interest in modeling and simulating the spacecraft electrical charging. This phenomenon is a source of in-orbit failures: energetic particles from the magnetospheric plasma interact with spacecraft, and these complex interactions can lead to high potential differences on the spacecraft surfaces. In turn, these potential differences induce the formation of electric arcing that can produce irreversible failures on the embarked devices, the solar arrays being a particularly sensible region. The problem has motivated the design of specific numerical codes in aerospace engineering: NASCAP and its evolution NASCAP-2K [22, 23], SPARCS [11], PicUp3D and SPIS [16,27], ESCAPE [24], SILECS [25,26] ... The specific modeling of the discharge phenomena and the electric arc formation is addressed e. g. in [3, 6, 7] where many references can be found; it splits into two steps: a primary discharge which creates connections and shortcuts between neighboring domains and a

Keywords and phrases: Vlasov-Poisson equations, Particles methods, Finite volume methods, Semi-lagrangian methods

[1] Project-Team SIMPAF, INRIA Lille Nord Europe Research Centre, 40 avenue Halley, Park Plazza, 59650 Villeneuve D'Ascq, France

[2] Current address: Laboratoire Jacques-Louis Lions, UMR 7598, UPMC, Université Paris 6, F-75005 Paris, France. e-mail: vauchelet@ann.jussieu.fr

[3] Thales Alenia Space, 100, bd. du Midi, 06156 Cannes La Bocca Cedex, France. e-mail: jean-paul.dudon@thalesaleniaspace.com

[4] Labo. Paul Painlevé UMR 8524 CNRS–Université des Sciences et Technologies de Lille. e-mail: christophe.besse@univ-lille1.fr & thierry.goudon@inria.fr

secondary arc characterized by the expansion of a plasma plume. The corresponding models usually use hydrodynamic systems which are beyond the scope of the present paper.

The in-orbit conditions make it reasonable to use a statistical description of the plasma surrounding the spacecraft. The charged particles interact with the electro-magnetic fields: the trajectories are influenced by the electromagnetic forces, which in turn are also modified by particles motion. To be more specific, in the geostationary orbits we are interested in, the mean free path remains large compared to the typical size characterizing the spacecraft and we can restrict to collisionless models. Furthermore, the effects of the magnetic field can be neglected and forces then reduce to the gradient of the electric potential. We are thus led to describe the plasma by Vlasov-Poisson equations. The charging phenomenom is driven by the boundary conditions which complete the equations: since the surface elements of the spacecraft have different dielectric properties, they have different sensibilities to the charge exchanges mechanisms and different behavior with respect to the potential variations. We shall see below that the boundary conditions to be used for in-orbit flight are highly non standard and lead to specific and challenging questions, both for mathematical analysis and numerical simulations.

The main source of numerical cost comes from the simulation of the Vlasov-type equation. It is costly due to the fact that the equation is set in phase space which means that we are working with three space variables and three velocity variables, additionally to the time variable. It already implies naturally a huge size of unknowns. Furthermore, the multiscale aspect of the problem may also lead to deal with stiff and delicate terms. In what follows, we shall consider three families of numerical methods to handle the problem:

- Particle-In-Cell (PIC) methods approach the plasma by a finite number of macroparticles (see [2, 14] for more details). The method consists in tracking the macroparticles along their trajectories, that is to compute the characteristics curves associated to the Vlasov equation. It adapts to 3D frameworks and allows to get satisfying results with relatively few particles. However, PIC methods are noisy, which can degrade the accuracy of the algorithm, see for instance the comments and currative attempts in [4, 26]. Moreover the computational time required seems to be very long.
- Another approach consists in discretizing the phase space, and interpreting the Vlasov equation as a conservation law in phase space, to propose a Finite Volume approximation (or flux balance method) [12, 17].
- Finally semi-lagrangian methods combine space phase discretization and integration along characteristics, through an interpolation step which is intended to project as smartly as possible the endpoint of the path on the grid after a time step. These methods usually provide an accurate approximation of the distribution function in the phase space [19].

It turns out that PIC methods have several advantages that make them well adapted for simulating spacecraft charging, and they are indeed widely used in industrial codes [11, 16, 22, 23, 25–27]. This is particularly relevant when considering geostationary orbits since the corresponding models do not need an accurate description of the particle distribution function. Instead, we can focus on the computation of the surface currents. For instance, the SPARCS code, which is currently in use at Thales Aleniaspace, is based on the Back-Trajectory method, which is a variant of PIC algorithms: we track the trajectories back from the points on the surface of the spacecraft until the trajectories reach the boundary where the distribution function is given. It allows to solve the Vlasov equation only on some particular points and make it interesting in that case. Besides, the software takes into account several physical phenomena like secondary emission, photo-emission and recollection of secondary electrons. Nevertheless, the recent development of Finite Volume and Semi Lagrangian methods, motivated e. g. from inertial or magnetic confinement fusion projects, see e. g. [15, 30] can make it relevant to consider these methods as potential alternative to the Back-Trajectory approach. Furthermore, spacecraft engineering is now concerned with a wide range of orbits where the physical conditions can significantly differ from the geostationary environment. Accordingly, we are led to more complex interaction models, which require a more accurate evaluation of the particles distribution function, including its spacial repartition far from the

spacecraft surface. Hence, we wish to compare the abilities of several numerical methods for solving the electric charge equations. To this end, we shall derive below a simple 1D model which contains the main difficulties of the actual problem. It will serve as a benchmark for discussing the pros and cons of the numerical methods. The paper is organized as follows. In the next Section, we introduce the model, with a detailed presentation of the boundary conditions on the spacecraft, in which the charging dynamics is embodied. In section 3, Vlasov solvers are presented and compared when the electrostatic potential E is assumed to be given. Finally, section 4 deals with the resolution of the whole model of spacecraft charging. An Appendix, which has its own interest, details the treatment of the boundary conditions when using the Semi-Lagrangian method.

1. Modeling of the spacecraft charging

1.1. **Description of the plasma**

The magnetospheric plasma is assumed to contain two charged particles species : ions H^+ and electrons. The distribution functions of these species are denoted by f_i and f_e respectively. At time t, $f_{i/e}(t,x,v)\ \mathrm{d}v\ \mathrm{d}x$ stands for the number of ions (respectively electrons) in the domain centered at the point (x,v) of the phase space with infinitesimal volume $\mathrm{d}v\ \mathrm{d}x$. We refer to [9–11] for a detailed discussion of the modeling issues for geostationary plasmas, which allow to neglect interparticles collisions and the effects of the magnetic field. Therefore, the distribution functions satisfy the Vlasov equation:

$$\partial_t f_{i/e} + v \cdot \nabla_x f_{i/e} + \frac{q_{i/e}}{m_{i/e}} \nabla_x \Phi \cdot \nabla_v f_{i/e} = 0, \tag{1}$$

where $q_i = -q_e = e > 0$, the elementary charge, m_i and m_e are respectively the ion mass and the electron mass. In this equation Φ denotes the selfconsistent electrostatic potential generated by the charged carriers. It is related to the macroscopic densities of charge by the Poisson equation

$$-\epsilon_0 \Delta_x \Phi = e(n_i - n_e), \tag{2}$$

where ε_0 is the vacuum permittivity and $n_{i/e}$ stand for the ion/electron density

$$n_{i/e}(t,x) = \int f_{i/e}(t,x,v)\ \mathrm{d}v.$$

Far from the satellite surfaces, the system is assumed to be at the equilibrium. It means that:

- The distribution functions are given by Maxwellians

$$\lim_{\|x\| \to +\infty} f_{i/e}(t,x,v) = g_{i/e}(v) = n_{0,i/e} \left(\frac{m_{i/e}}{2\pi k T_{i/e}} \right)^{3/2} \exp\left(-\frac{m_{i/e} v^2}{2 k T_{i/e}} \right),$$

  where $n_{0,i/e}$ is the given number density and $T_{i/e}$ the temperature of the distribution of particles, k being the Boltzmann constant;
- The electrostatic potential vanishes at infinity

$$\lim_{\|x\| \to +\infty} \Phi(t,x) = 0.$$

The derivation of the boundary condition on the spacecraft is more subtle. The external surfaces of the spacecraft are subject to the current

$$J_{ext}(t,x) = e \int v (f_i - f_e)(t,x,v)\ \mathrm{d}v$$

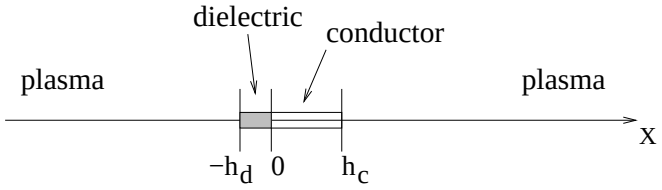

FIGURE 1. Scheme of the spacecraft.

due to the charged particles of the plasma. This current induces a modification of the electrostatic potential on the boundary of the spacecraft. Indeed the Ampère equation furnishes the evolution in time of the electrostatic potential:

$$\epsilon_0 \frac{\partial}{\partial t}\frac{\partial \Phi}{\partial \nu} - J_{ext}\cdot\nu = 0, \tag{3}$$

at the boundary between the spacecraft and the plasma where $\nu(x)$ stands for the outward unit vector at a point x of the spacecraft boundary. It is completed by boundary conditions for the charged particles distribution that take into account reflection of the impinging particles, various emission phenomena with different energy spectrum, as well as recollection of secondary electrons. The originality of this model is that these boundary conditions are time-dependent with a time derivative. The derivation of the evolution equations at the boundary will be clarified in the next section.

Let us make a short break on scaling issues, still referring to [9–11, 26]. In geostationary orbits, the Debye length is large with respect to the characteristic length of a spacecraft. Accordingly, asymptotic arguments allow to get rid of the time derivative in (1) and to assume quasi-neutrality. Hence, (1)-(2) can be replaced in this situation by the system

$$\begin{cases} v\cdot\nabla_x f_{i/e} + \dfrac{q_{i/e}}{m_{i/e}}\nabla_x\Phi\cdot\nabla_v f_{i/e} = 0, \\ \\ \Delta\Phi = 0. \end{cases} \tag{4}$$

However, the scaling does not disregard the time derivative in the boundary conditions for the potential (3). Hence, the time variable appears as a parameter in the stationary Vlasov-Laplace system, and the evolution of the charging phenomena is governed by the non stationary boundary conditions at the spacecraft surface. Such approximated models are used in several codes [11, 23, 26].

1.2. **One-dimension model**

Let us now derive a one-dimension caricature of the spacecraft charging model. The simplified model is intended to exhibit the main features of the actual equations, in particular the evolution terms arising in the boundary conditions. Having at hand such a toy model allows to point out easily the difficulties of the model as well as to evaluate the advantages and drawbacks of numerical methods. It can be seen as a necessary step to extend the simulations in higher dimension.

Since we are mainly concerned with numerical purposes, we consider a bounded domain, characterized by $0 < L < \infty$. The spacecraft is seen as an assembly of a dielectric layer and a metallic conductor. We consider that the conductor occupies the interval $[0, h_c]$ whereas the dielectric takes place in $[-h_d, 0)$ (see Figure 1). Therefore h_d denotes the thickness of the dielectric layer and h_c the width of the conductor. Hence, the plasma fills the domain $]-L-h_d, -h_d[\cup]h_c, L+h_c[$. According to the previous Section, we use the following 1D version of the Vlasov-Poisson system:

$$\partial_t f_{i/e} + v\cdot\partial_x f_{i/e} + \frac{q_{i/e}}{m_{i/e}}\partial_x\Phi\cdot\partial_v f_{i/e} = 0, \qquad t>0,\ x\in]-L-h_d,-h_d[\cup]h_c,L+h_c[,\ v\in\mathbb{R}. \tag{5}$$

where the electrostatic field $E = -\partial_x \Phi$ is calculated thanks to the Poisson equation :

$$\left\{ \begin{array}{l} -\epsilon_0 \, \partial^2_{xx} \Phi = e(n_i - n_e) = \displaystyle\int_{\mathbb{R}} e(f_i - f_e) \, \mathrm{d}v, \qquad x \in]-L-h_d, -h_d[\cup]h_c, L+h_c[. \end{array} \right. \tag{6}$$

At the initial time, the system is assumed to be not perturbed and the distribution functions are given by the Maxwellian distribution :

$$f_{i/e}(0,x,v) = n_{0,i/e} \sqrt{\frac{m_{i/e}}{2\pi k T_{i/e}}} \exp\left(-\frac{m_{i/e} v^2}{2 k T_{i/e}} \right). \tag{7}$$

At the external boundary, bearing in mind that L is a cut-off parameter to be chosen large enough, we use the equilibrium as incoming boundary conditions:

$$\left\{ \begin{array}{ll} f_{i/e}(t, -L-h_d, v) = n_{0,i/e} \sqrt{\dfrac{m_{i/e}}{2\pi k T_{i/e}}} \exp\left(-\dfrac{m_{i/e} v^2}{2 k T_{i/e}} \right), & \text{for } v > 0, \\ f_{i/e}(t, L+h_c, v) = n_{0,i/e} \sqrt{\dfrac{m_{i/e}}{2\pi k T_{i/e}}} \exp\left(-\dfrac{m_{i/e} v^2}{2 k T_{i/e}} \right), & \text{for } v < 0. \end{array} \right. \tag{8}$$

while for the potential we get

$$\Phi(-L-h_d) = \Phi(L+h_c) = 0. \tag{9}$$

At the spacecraft boundary, we assume that particles are specularly reflected

$$\left\{ \begin{array}{l} f_{i/e}(t, -h_d, v) = \alpha \; f_{i/e}(t, -h_d, -v) \;\; \text{if} \;\; v < 0, \\ f_{i/e}(t, h_c, v) = \alpha \; f_{i/e}(t, h_c, -v) \;\; \text{if} \;\; v > 0, \end{array} \right. \tag{10}$$

with $0 \leq \alpha \leq 1$ a parameter measuring the proportion of reflected particles. It thus remains to discuss the boundary conditions on $-h_d$ and h_c for the potential. These boundary conditions will connect the behavior of the plasma in the two intervals $(-L-h_d, -h_d)$ and $(h_c, L+h_c)$.

To this end, it is convenient to introduce a reference potential Φ_{ref} which corresponds to the potential created by a scatterer occupying $(-h_d, h_c)$ and charged uniformly. The reference charge being fixed to $1V$, Φ_{ref} is defined by

$$\left\{ \begin{array}{l} \partial^2_{xx} \Phi_{ref} = 0, \\ \Phi_{ref}(-h_d) = \Phi_{ref}(h_c) = 1, \qquad \Phi_{ref}(L+h_c) = \Phi_{ref}(-L-h_d) = 0. \end{array} \right. \tag{11}$$

Next, in a perfect conductor the potential remains constant at any place. Hence, let us denote by $\phi_{abs}(t)$, the so–called absolute potential, the value of the potential in $[0, h_c]$:

$$\Phi(t,x) = \phi_{abs}(t), \qquad \text{for all } x \in [0, h_c].$$

This value is of course still to be determined. Then, we write

$$\Phi(t,x) = \phi_{abs}(t) \, \Phi_{ref}(x) + \Phi'(t,x), \tag{12}$$

which defines the differential potential Φ'. Thanks to (6) and (11), we deduce that the differential potential Φ' satisfies :

$$\left\{ \begin{array}{l} -\epsilon_0 \, \partial^2_{xx} \Phi'(t,x) = e(n_i - n_e), \\ \Phi'(t, L+h_c) = \Phi'(t, -L-h_d) = 0, \\ \Phi'(t, h_c) = 0. \end{array} \right. \tag{13}$$

We are thus left with the task of defining conditions for ϕ_{abs} and $\Phi'(t, -h_d)$.

1.3. **Charging evolution**

Actually, the electrostatic field $E = -\partial_x \Phi$ is defined in the whole domain

$$]-L-h_d, -h_d[\cup[-h_d, 0[\cup[0, h_c]\cup]h_c, L+h_c[,$$

where the four intervals correspond to different physical properties (that is vacuum, dielectric, conductor, vacuum). On the one hand, at any place, $E = -\partial_x \Phi$ satisfies the equation

$$\epsilon\, \partial_x E = \rho,$$

where ϵ is the permittivity, depending on the medium, and ρ is the density of charge. On the other hand, the charge conservation

$$\partial_t \rho + \partial_x J = 0,$$

holds where J is the current density. In the plasma domain $]-L-h_d, -h_d[\cup]h_c, L+h_c[$, we have

$$\rho = e(n_i - n_e), \qquad J = e\int_{\mathbb{R}} v(f_i - f_e)\ \mathrm{d}v,$$

and the continuity equation follows by integrating with respect to v the Vlasov equations. Therefore, we have

$$\epsilon\, \partial_t \partial_x E + \partial_x J = 0.$$

Since this relation must be satisfied in all the domain $(-L-h_d, L+h_c)$, it yields jump conditions at each boundary

$$-\frac{\partial}{\partial t}\left[\epsilon \frac{\partial \Phi}{\partial x}\right] + [J] = 0, \tag{14}$$

where $[.]$ denotes the jump at the interfaces.

Let us denote by J_{ext} the net current on the spacecraft from the plasma, that is

$$J_{ext}(t, h_c) = e\int_{\mathbb{R}} v(f_i - f_e)(t, h_c, v)\ \mathrm{d}v$$
$$J_{ext}(t, -h_d) = e\int_{\mathbb{R}} v(f_i - f_e)(t, -h_d, v)\ \mathrm{d}v$$

In view of the boundary condition (10), it reads

$$J_{ext}(t, h_c) = (1-\alpha)\ e\int_{v<0} v(f_i - f_e)(t, h_c, v)\ \mathrm{d}v$$
$$J_{ext}(t, -h_d) = (1-\alpha)\ e\int_{v>0} v(f_i - f_e)(t, -h_d, v)\ \mathrm{d}v.$$

The current inside the conductor is denoted J_{cond}. We recall that in the conductor the electrostatic potential keeps a constant value denoted ϕ_{abs}. We make the assumption that the dielectric layer is very thin, $h_d \ll 1$, so that there is no volumic charge in the dielectric and the derivative of the potential in the dielectric can be approximated by the finite difference

$$\frac{\partial \Phi}{\partial x} \simeq \frac{\phi_{abs} - \Phi(-h_d)}{h_d}.$$

Finally there exists a runaway current between the dielectric and the conductor, which is proportional to the difference of potential, see [21],

$$J_{diel} = -\sigma_d \frac{\phi_{abs} - \Phi(-h_d)}{h_d},$$

σ_d being the conductivity of the dielectric. Therefore, the jump relations read as follows

- At the interface $x = -h_d$ between the plasma and the dielectric

$$\partial_t \left(\epsilon_0 \partial_x \Phi(-h_d) - \epsilon_d \frac{\phi_{abs} - \Phi(-h_d)}{h_d} \right) = J_{ext}(-h_d) + \sigma_d \frac{\phi_{abs} - \Phi(-h_d)}{h_d}. \tag{15}$$

- At the interface $x = 0$ between the dielectric and the conductor

$$\partial_t \left(\epsilon_d \frac{\phi_{abs} - \Phi(-h_d)}{h_d} \right) = -\sigma_d \frac{\phi_{abs} - \Phi(-h_d)}{h_d} - J_{cond}. \tag{16}$$

- At the interface $x = -h_c$ between the conductor and the plasma

$$-\partial_t(\epsilon_0 \partial_x \Phi(h_c)) = J_{cond} - J_{ext}(h_c). \tag{17}$$

We get rid of the unknown J_{cond} by summing equation (16) with (17) which yields

$$\partial_t \left(\epsilon_d \frac{\phi_{abs} - \Phi(-h_d)}{h_d} - \epsilon_0 \partial_x \Phi(h_c) \right) = -\sigma_d \frac{\phi_{abs} - \Phi(-h_d)}{h_d} - J_{ext}(h_c).$$

We can finally sum this last relation with (15) to obtain

$$\epsilon_0 \partial_t \partial_x (\Phi(-h_d) - \Phi(h_c)) = J_{ext}(-h_d) - J_{ext}(h_c). \tag{18}$$

Furthermore (15) can be rewritten, using the definition of Φ' in (12),

$$\epsilon_0 \partial_t \partial_x \Phi(-h_d) + \frac{\epsilon_d}{h_d} \partial_t \Phi'(-h_d) + \frac{\sigma_d}{h_d} \Phi'(-h_d) = J_{ext}(-h_d). \tag{19}$$

The two identities (18) and (19) are evolution equations which define the two quantities $\Phi'(-h_d)$ and ϕ_{abs}. Therefore the Vlasov-Poisson system (5)–(10) is completed with the boundary conditions for the potential :

$$\Phi(t, h_c) = \phi_{abs}(t) \ ; \qquad \Phi(t, -h_d) = \phi_{abs}(t) + \Phi'(t, -h_d). \tag{20}$$

1.4. **Asymptotic issues**

We set $\delta = h_d/h_c$, $V_e = \sqrt{kT_e/m_e}$, the thermal velocity of the electrons, $\Phi_0 = m_e V_e^2/e$. We introduce typical value for the density $n_{0,e}$, and we define $J_0 = e n_{0,e} V_e$, and $T_0 = \dfrac{\epsilon_0 \Phi_0}{J_0 h_d}$, the typical time of charging of the dielectric. We define the dimensionless quantities :

$$\widetilde{\Phi} = \frac{\Phi}{\Phi_0}, \ \widetilde{J} = \frac{J}{J_0}, \ \widetilde{x} = \frac{x}{h_c}, \widetilde{t} = \frac{t}{T_0}.$$

Therefore equations (18) and (19) in dimensionless form become

$$\delta \partial_{\tilde{t}} \partial_{\tilde{x}} (\widetilde{\Phi}(-h_d) - \widetilde{\Phi}(h_c)) = \widetilde{J_{ext}}(-h_d) - \widetilde{J_{ext}}(h_c),$$

$$\delta \partial_{\tilde{t}} \partial_{\tilde{x}} \widetilde{\Phi}(-h_d) + \frac{\epsilon_d}{\epsilon_0} \partial_{\tilde{t}} \widetilde{\Phi'}(-h_d) + \frac{\sigma_d}{h_d} \frac{m_e V_e}{e^2 n_{0,e}} \widetilde{\Phi'}(-h_d) = \widetilde{J_{ext}}(-h_d).$$

As already said the dielectric layer is very thin, and in applications we are interested in the case $0 < \delta \ll 1$. Thus, from now on we will formally neglect the term with δ in factor. Finally, the equations on the unknowns $\Phi'(-h_d)$ and ϕ_{abs} are

$$J_{ext}(-h_d) = J_{ext}(h_c), \tag{21}$$

$$C_d \frac{\mathrm{d}}{\mathrm{d}t}\Phi'(-h_d) + S_d \Phi'(-h_d) = J_{ext}(-h_d), \tag{22}$$

where C_d is the given capacity and S_d the conductance of the dielectric.

Let us recap the 1D model we will use for describing the evolution of the charge at the external surface of the spacecraft. The distribution function f_i and f_e are solutions for $x \in]-L-h_d, h_d[\cup]h_c, L+h_c[$ and $v \in \mathbb{R}$ of the Vlasov equation

$$\partial_t f_{i/e} + v \cdot \partial_x f_{i/e} + \frac{q_{i/e}}{m_{i/e}} \partial_x \Phi \cdot \partial_v f_{i/e} = 0, \qquad t > 0,$$

completed with the initial condition

$$f_{i/e}(0,x,v) = n_{0,i/e} \sqrt{\frac{m_{i/e}}{2\pi k T_{i/e}}} \exp\left(-\frac{m_{i/e} v^2}{2kT_{i/e}}\right),$$

and the boundary conditions (with $0 \le \alpha \le 1$)

$$\begin{cases} f_{i/e}(t,-h_d,v) = \alpha\ f_{i/e}(t,-h_d,-v), & \text{for } \ v<0, \\ f_{i/e}(t,h_c,v) = \alpha\ f_{i/e}(t,h_c,-v), & \text{for } \ v>0, \\ f_{i/e}(t,-L-h_d,v) = n_{0,i/e}\sqrt{\dfrac{m_{i/e}}{2\pi k T_{i/e}}} \exp\left(-\dfrac{m_{i/e} v^2}{2kT_{i/e}}\right), & \text{for } v>0, \\ f_{i/e}(t,L+h_c,v) = n_{0,i/e}\sqrt{\dfrac{m_{i/e}}{2\pi k T_{i/e}}} \exp\left(-\dfrac{m_{i/e} v^2}{2kT_{i/e}}\right), & \text{for } v<0. \end{cases}$$

The electrostatic potential Φ is calculated thanks to the Poisson problem :

$$\begin{cases} -\epsilon_0 \partial^2_{xx}\Phi = e(n_i - n_e) = \displaystyle\int_{\mathbb{R}} e(f_i - f_e)\ \mathrm{d}v, \qquad x \in]-L-h_d, -h_d[\cup]h_c, L+h_c[, \\ \Phi(-L-h_d) = \Phi(L+h_c) = 0, \\ \Phi(h_c) = \phi_{abs}, \qquad \Phi(-h_d) = \phi_{abs} + \Phi'(-h_d). \end{cases}$$

Eventually, given

$$\begin{aligned} J_{ext}(t,-h_d) &= (1-\alpha)\ e \int_{v>0} (f_i(t,-h_d,v) - f_e(t,-h_d,v))\ \mathrm{d}v, \\ J_{ext}(t,h_c) &= (1-\alpha)\ e \int_{v<0} (f_i(t,h_c,v) - f_e(t,h_c,v))\ \mathrm{d}v, \end{aligned} \tag{23}$$

ϕ_{abs} and $\Phi'(t,-h_d)$ are determined by

$$\begin{aligned} &J_{ext}(-h_d) = J_{ext}(h_c), \\ &C_d \frac{\mathrm{d}}{\mathrm{d}t}\Phi'(-h_d) + S_d \Phi'(-h_d) = J_{ext}(-h_d). \end{aligned} \tag{24}$$

Even in the mere 1D framework, this model is highly non standard; its mathematical analysis is certainly tough and it provides an already challenging test for numerical simulations.

Remark 1. *In the case of total reflection $\alpha = 1$, the external current vanishes on the boundaries $J_{ext}(t, -h_d) = 0 = J_{ext}(t, h_c)$. Accordingly, the differential potential on the dielectric $\Phi'(t, -h_d)$ vanishes exponentially fast (or stays at zero if it is initially) and the absolute potential ϕ_{abs} remains constant; there is no charging, in agreement to the physical intuition.*

1.5. **Towards multi-dimensional problems**

Of course, realistic simulations are performed in a 3 dimensional framework. The basic equations are still (1)-(2), or, if scaling properties applies like in GEO, we can use (4). The latter has the advantage of disregarding any volume effects, focusing on variations of charge due to surface phenomena. The boundary conditions at infinity for the particle distribution functions and the potential are at equilibrium. The geometry makes more involved the boundary conditions on the spacecraft. As said above the charged particles are subject to complicated phenomena which determine the absorption/emission and reflection laws to be used on the spacecraft boundary and which define the incoming distribution. Clearly, surfaces with different components yield different reflection laws, and the derivation of these boundary conditions is mainly based on phenomelogical arguments. The main difficulty however is related to the condition satisfied by the potential.

The derivation proposed in [9] is based on the study of jump relations on the interfaces between the different domains: plasma, dielectric, conductor. This is the approach we followed for obtaining the one-dimension problem. The spacecraft is seen as a perfect conductor, partially covered by an assembly of dielectric materials. We denote by $\mathcal{O}_0$ the conductor, and $\mathcal{O}_k$, $k \in \{1, ..., N_d\}$ the dielectrics which are characterized by their permittivity $\varepsilon_k > 0$ and conductivity $\sigma_k > 0$. The height of the kth dielectric layer is denoted by h_k. The plasma fills the domain $\Omega = \mathbb{R}^3 \setminus \overline{\bigcup_{k=0}^{N_d} \mathcal{O}_k}$. We set $\Gamma = \bigcup_{k=0}^{N_d} \partial\mathcal{O}_k$ and for a given point $x \in \Gamma$, $\nu(x)$ stands the outward normal vector at the surface Γ. We consider the following interfaces (see figure 2):

- $\Gamma_{c/v} = \Gamma \setminus \bigcap_{k=0}^{N_d} \partial\mathcal{O}_k$ the interface between the conductor and the vacuum,
- $\Gamma_{c/d} = \partial\mathcal{O}_0 \setminus \Gamma_{c/v}$ the interface between the conductor and the dielectrics,
- $\Gamma_{d/v} = \partial\Omega \setminus \Gamma_{c/v}$ the interface between the dielectrics and the vacuum,
- $\Gamma_{d/d} = \Gamma \setminus (\partial\mathcal{O}_0 \cup \partial\Omega)$ the interface between neighbors dielectrics.

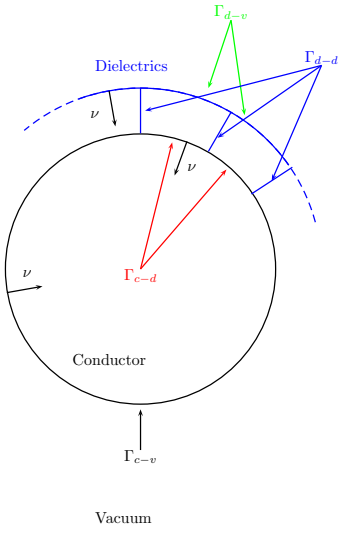

FIGURE 2. Domain and notations of interfaces

At any place of the conductor, the electric potential remains at a constant value: $\phi_{abs}(t)$, the so-called "absolute potential". In particular, we have

$$\Phi(t,x) = \phi_{abs}(t) \text{ on } \Gamma_{c/v}. \tag{25}$$

In the dielectrics, the runaway current is proportional to the electric field $J_k = -\sigma_k \nabla_x \Phi_{diel}$. Then, we consider the jump relations associated to the Ampère law: denoting $J_{ext} = J_i + J_e$, we get

$$\partial_t(\epsilon_k \partial_\nu \Phi_{diel} - \epsilon_0 \partial_\nu \Phi) + J_{ext} \cdot \nu + \sigma_k \partial_\nu \Phi_{diel} = 0 \quad \text{ on } \Gamma_{d/v} \tag{26}$$

and

$$\int_{\Gamma_{c/v}} \Big[\partial_t(-\epsilon_0 \partial_\nu \Phi) + J_{ext} \cdot \nu\Big] \ \mathrm{d}\gamma + \int_{\Gamma_{c/d}} \Big[\partial_t(-\epsilon_k \partial_\nu \Phi_{diel}) - \sigma_k \partial_\nu \Phi_{diel}\Big] \ \mathrm{d}\gamma = 0. \tag{27}$$

Since the dielectric layer is very thin, which means that the h_k's are small compared to the characteristic lengths of the spacecraft, the normal derivative of the dielectric potential on $\Gamma_{c/d}$ and $\Gamma_{d/v}$ is approached by

$$\partial_\nu \Phi_{diel}(t,x) \simeq \frac{\phi_{abs}(t) - \Phi(t,x)}{h_k}. \tag{28}$$

Finally (25), (26), (27) and (28) defines the boundary conditions for the potential. A further scaling argument leads to replace (26)–(27) by

$$C_k \partial_t\big(\phi_{abs}(t) - \Phi(t,x)\big) + S_k\big(\phi_{abs}(t) - \Phi(t,x)\big) = -J_{ext} \cdot \nu \quad \text{ on } \Gamma_{d/v}$$

together with the constraint

$$\int_{\Gamma_{c/v} \cup \Gamma_{c/v}} J_{ext} \cdot \nu \ \mathrm{d}\gamma = 0,$$

where C_k and S_k are respectively the capacity and conductance per unit area of the dielectric.

The current version of SPARCS uses these boundary conditions. However, the adopted modeling is intimately related to the numerical methods and alternative approaches are possible. A possibility is to compute the electric field everywhere. Taking into account the complex structure of the spacecraft would require the use of a very fine mesh, at the size of the thickness of the dielectrics, together with a detailed description of the electrical phenomena in each domain, which is in general not affordable. Another strategy defines a charge repartition on the surface of the spacecraft by using a suitable charge distribution technique which is intended to account for the complex electric network constituted by the different materials. Hence, the issue of boundary conditions for the potential is converted into a definition of virtual charges to be distributed on the spacecraft. This is done either by the so–called Capacitance Matrix Method [3, 16, 26] or by defining an equivalent circuit [16, 22, 23].

2. Presentation of Vlasov solvers

Clearly, having in mind applications to spacecraft engineering, computational time and memory size consumption will be crucial criteria addressed on numerical schemes.

2.1. **Some properties of the Vlasov equation**

We first recall briefly some well known properties of the Vlasov equation. Indeed, the numerical methods for solving the Vlasov equation :

$$\frac{\partial f}{\partial t}(t,x,v) + v \cdot \partial_x f(t,x,v) - \frac{q}{m} E(t,x) \cdot \partial_v f(t,x,v) = 0, \tag{29}$$

relies

- either on this non conservative form of the equation, which appeals (neglecting any difficulty related to the regularity of the potential) to define the characteristics curves by the ODE system:

$$\begin{cases} \dfrac{\mathrm{d}X}{\mathrm{d}s}(s;x,v,t) = V(s;x,v,t), & X(t;x,v,t) = x, \\ \dfrac{\mathrm{d}V}{\mathrm{d}s}(s;x,v,t) = -\dfrac{q}{m}E(s,X(s;x,v,t)), & V(t;x,v,t) = v \end{cases}. \tag{30}$$

  Hence (29) means that particles are conserved along the characteristics

$$\frac{\mathrm{d}}{\mathrm{d}s}\big[f(s,X(s;x,v,t),V(s;x,v,t))\big] = 0,$$

  or, in other words

$$f(t,x,v) = f(s,X(s;x,v,t),V(s;x,v,t)), \qquad \forall\, s \geq 0.$$

  This property is at the basis of semi-lagrangian and particle methods.
- or we note that $\mathrm{div}_{x,v}(v,-\frac{q}{m}E) = 0$ and we rewrite the equation on the conservative form

$$\frac{\partial f}{\partial t}(t,x,v) + \partial_x\big(v f(t,x,v)\big) - \partial_v\big(\frac{q}{m}E(t,x)f(t,x,v)\big) = 0$$

  which appeals to the finite volume framework developed for the simulation of conservation laws [20].

2.2. **Finite volume**

The Vlasov equation recasts in the conservative form

$$\partial_t f + \mathrm{div}_{(x,v)}(\mathbf{U}(t,x,v)f) = 0,$$

where $\mathbf{U}(t,\cdot,\cdot) : \mathbb{R}^2 \to \mathbb{R}^2$, $(x,v) \mapsto (v,-\frac{q}{m}E)$. The phase space domain (x,v) is meshed by the nodes $(x_i)_{1\leq i\leq N_x}$ and $(v_j)_{1\leq j\leq N_v}$, with mesh steps Δx and Δv respectively. The control volume is denoted by $C_{i,j} = [x_i, x_{i+1}] \times [v_j, v_{j+1}]$. Integrating the Vlasov equation (29) on $(t^n, t^{n+1}) \times C_{i,j}$ yields

$$\begin{aligned} &\int_{C_{ij}} f(t^{n+1},x,v)\ \mathrm{d}v\ \mathrm{d}x - \int_{C_{ij}} f(t^n,x,v)\ \mathrm{d}v\ \mathrm{d}x \\ &= -\int_{t^n}^{t^{n+1}} \int_{v_j}^{v_{j+1}} v(f(s,x_{i+1},v) - f(s,x_i,v))\ \mathrm{d}v\ \mathrm{d}s \\ &+ \int_{t^n}^{t^{n+1}} \int_{x_i}^{x_{i+1}} \frac{q}{m}E(s,x)(f(s,x,v_{j+1}) - f(s,x,v_j))\ \mathrm{d}x\ \mathrm{d}s. \end{aligned} \tag{31}$$

Therefore, the discrete unknown f_{ij}^n is intended to be an approximation of the average value at time t^n on the cell C_{ij}, that is $\frac{1}{\Delta x\ \Delta v}\int_{C_{i,j}} f(t^n,x,v)\ \mathrm{d}x\ \mathrm{d}v$ and finite volume methods are based on the determination of fluxes on the volume interfaces to construct an iterative procedure inspired from (31). Namely, the scheme can be written as

$$f_{i,j}^{n+1} = f_{i,j}^n - \frac{\Delta t}{\Delta x}\big(\mathcal{F}_{i+1/2,j}^n - \mathcal{F}_{i-1/2,j}^n\big) + \frac{\Delta t}{\Delta v}\big(\mathcal{G}_{i,j+1/2}^n - \mathcal{G}_{i,j-1/2}^n\big). \tag{32}$$

We use a time–explicit scheme since the fluxes in the right hand side only depend on the values of the unknown at time t^n. The fluxes at the interface of the control volume C_{ij} are determined by using the reconstruction method presented in [12] based on the second order PFC method [17]. We set

$$f_{i+1/2,j}^n = \frac{1}{2}(f_{i,j}^n + f_{i+1,j}^n)\ , \qquad f_{i,j+1/2}^n = \frac{1}{2}(f_{i,j}^n + f_{i,j+1}^n).$$

Let $\tilde{E}_i^n$ be an approximation of $E(t^n, x)$ for $x \in [x_i, x_{i+1})$ computed through the resolution of the Poisson equation. Then, we get in (32)

$$\mathcal{F}_{i+1/2,j}^n = v_j \; f_{i+1/2,j}^n, \qquad \mathcal{G}_{i,j+1/2}^n = \tilde{E}_i^n \; f_{i,j+1/2}^n.$$

However, this second order approximation reconstruction method can generate spurious oscillations since we obtain then a classical centered scheme. Therefore a slope corrector, ensuring the positivity of the distribution function, has been introduced in [12]. The final scheme is then given in equation (3.6) of [12].

Eventually, in order to guaranty the stability of the scheme, a CFL condition has to be imposed on the time step (see Proposition 3.2 of [12]) ensuring the positivity of the distribution function :

$$\Delta t \leq \max\left(\frac{\Delta x}{V_{max}}, \frac{\Delta v}{E_{max}}\right),$$

where E_{max} is the maximum value of the electric field E_{max} and V_{max} is the bound of the velocity domain. This CFL condition can be very restrictive and even prohibitive for the application treated here. Indeed, for geostationary orbits, the thermal velocity for electrons is $V_e = 4.5\,10^7 m.s^{-1}$. Choosing $V_{max} = 2V_e$, the CFL condition imposes a time step Δt lesser than 10^{-8} s ! The complexity of this algorithm for each time step is $O(N_x N_v)$.

2.3. **Semi-lagrangian methods**

These methods consist in calculating the distribution function at time $t^{n+1} = t^n + \Delta t$ thanks to the one which has been obtained at the time t^n by using the conservation relation along the characteristics curves (see section 2.1). It thus relies on a discrete approximation of the relation

$$f(t^n + \Delta t, x_i, v_j) = f(t^n, X(t^n; x_i, v_j, t^n + \Delta t), V(t^n; x_i, v_j, t^n + \Delta t))$$

where the notations are defined in (30). Therefore two main steps are necessary :

(1) Find the point $(X(t^n; x_i, v_j, t^n + \Delta t), V(t^n; x_i, v_j, t^n + \Delta t) = (X^n, V^n)$. Starting from (x_i, v_j), it suffices to go back along the characteristics curves during the time step Δt. To this end, we have to solve (30). This resolution is splitted into three steps [1, 13, 29] :

- backward advection of $\Delta t/2$ in the spatial direction :

$$X^{n+1/2} = X^{n+1} - \frac{\Delta t}{2} V^{n+1} = x_i - \frac{\Delta t}{2} v_j.$$

- backward advection of Δt in the velocity direction :

$$V^n = V^{n+1} + \Delta t \frac{q}{m} E(t^{n+1/2}, X^{n+1/2}).$$

- backward advection of $\Delta t/2$ in the spatial direction :

$$X^n = X^{n+1/2} - \frac{\Delta t}{2} V^n.$$

Obviously, if the trajectory reaches a boundary $x = -h_d$ or $x = h_c$, then we use specular reflexion : V^n is replaced by its opposite and X^n by its symmetric. More precisely, if for instance $X^{n+1/2} < -L - h_d$ and $X^n > -L - h_d$, then

$$t_{sym} := \frac{X^{n+1} + L + h_d}{-V^{n+1}}, \qquad X^{n+1/2} = -L - h_d - t_{sym} V^{n+1},$$
$$V^n = -V^{n+1} + \Delta t \frac{q}{m} E(t^{n+1/2}, X^{n+1/2}), \qquad X^n = X^{n+1/2} - \frac{\Delta t}{2} V^n.$$

The value $E(t^{n+1/2}, X^{n+1/2})$ is computed by a linear interpolation.

(2) Since f at time t^n is known only on the nodes of the mesh, we interpolate the distribution function at the point $(X(t^n; t^n + \Delta t, x_i, v_j), V(t^n; t^n + \Delta t, x_i, v_j))$. We use a Hermite spline interpolation which is a well established high order interpolation method. We refer e. g. to [13, 29] for details on this interpolation step, an alternative approach based on the WENO procedure has been proposed recently in [8]. However, most of the references we are aware of restrict to periodic boundary conditions and do not address the question of the interpolation rule to be adopted for boundary points. We give some hints in this direction in the Appendix, this aspect being important to preserve the accuracy of the numerical scheme.

Although the high order of the interpolation step allows to obtain a good numerical accuracy, this step is also highly time and memory consuming. Indeed, each time step involves the inversion of $N_v + 1$ matrices of size $(N_x + 3) \times (N_x + 3)$ and $N_x + 3$ matrices of size $(N_v + 3) \times (N_v + 3)$. Moreover, for memory size reasons, we impose that the trajectories do not cross over more than 2 or 3 cells of the mesh during a time step. It implies a constraint on the time step $\Delta t \leq 2\,\Delta x/V_{max}$ which is yet less restrictive than the CFL condition for the finite volume method. The complexity is of the same order than for the finite volume method : each time step requires $O(N_x N_v)$ operations. In fact, the construction of the spline basis and therefore the LU decomposition of the $N_x + 3 + N_v + 1$ matrices is done only once at the beginning of the procedure and demands therefore $O(N_x N_v)$ operations. Then $N_x \times N_v$ interpolations are necessary. We underline finally that due to the memory size required, this method is not affordable for 3D simulations.

2.4. **Back-Trajectory method**

This method is a Particle In Cell (PIC) type method [5]. Like with a standard PIC method, the plasma is approximated by a finite number of macroparticles. Each macroparticle is tracked backward its trajectory [9,11]. More precisely, we use the conservation relation along the characteristics curves again and we distinguish two situations:

- Either the trajectory reaches the external boundary at time $s_\infty > 0$ with position, velocity pair $(X(s_\infty; x, v, t), V(s_\infty; x, v, t))$. We remind that the external boundary is fixed far from the spacecraft and the data f_∞ there is intended to reproduce the equilibrium at infinity of the original model. We get
$$f(t, x, v) = f_\infty(X(s_\infty; x, v, t), V(s_\infty; x, v, t)).$$
- or we set
$$f(t, x, v) = f_0(X(0; x, v, t), V(0; x, v, t)), \tag{33}$$
where f_0 is the given initial distribution function.

Thus the main step of the algorithm consists in computing the origin of the characteristics $(X(0; x, v, t), V(0; x, v, t))$ or $(X(s_\infty; x, v, t), V(s_\infty; x, v, t))$ which reaches (x, v) at time t. We use an implicit-explicit discretization of (30) (see [14])). To compute the distribution function at time $t^N = N\Delta t$, $N \in \mathbb{N}^*$, at node $(x, v) = (X^N, V^N)$, we track the characteristics back in time with the scheme

$$\begin{cases} \dfrac{X^{i+1} - X^i}{\Delta t} = -V^{i+1} & ; \quad X^N = x, \\ \dfrac{V^{i+1} - V^i}{\Delta t} = \dfrac{q}{m} E(t^i, X^i) & ; \quad V^N = v, \end{cases}$$

for $i = N-1, N-2, \cdots$ Three cases can occur. If the trajectory reaches a boundary of the satellite, we use the specular reflection law (10) and the computation continues. If the trajectory goes to the external boundary, the solution is given by the Maxwellian at infinity in (7). Otherwise after N iterations in time we have computed the values of $X(0; x, v, t^N)$ and $V(0; x, v, t^N)$ which allows to determine f thanks to (33).

Once the distribution function f is computed, the current at the point x is obtained thanks to a discretization of the integral :

$$J(t,x) = q\int_{\mathbb{R}} vf(t,x,v)\ \mathrm{d}v = \sum_k \alpha^k q \left(\int_{B_k(t,x)} vf_0(X(0;x,v,t),V(0;x,v,t))\ \mathrm{d}v + \int_{A_k(t,x)} vf_\infty(X(s_\infty;x,v,t),V(s_\infty;x,v,t))\ \mathrm{d}v \right), \tag{34}$$

where $A_k(t,x)$ (resp. $B_k(t,x)$) is the set of velocities $v \in \mathbb{R}$ for which the trajectory reaching (x,v) at time t comes from the external ("infinity") boundary (resp. from a point located inside the domain at time 0) after k hits on the boundary.

The main advantage of this approach is that it is possible to disregard the volume filled by the plasma, but instead to focus on the boundary. This is well adapted to the geostationary environment, where we use the simplified model (4). In this case, the right hand side of the Poisson equation is zero, then the Vlasov equation is solved only to compute the external current J_{ext} at the boundaries $x = -h_c$ and $x = h_d$. By using the BackTrajectory method we can compute the distribution function on the nodes of the boundary without the knowledge of the distribution function in the entire domain. Moreover, no constraint on the time step is necessary to insure the stability and the dynamical allocation of memory stays moderate such that we can easily extend to the 3D framework. At each time step $N_x \times N_v$ trajectories are calculated. Each trajectory which do not reach the external boundary demands $O(N)$ operations. Therefore the number of operations increases with time. However due to the finite number of macroparticles used, these methods are known to be extremely noisy, a difficulty which becomes sensible for long time simulations. In fact, a small modification of the issue (x,v) of the characteristics can modify a trajectory such that v moves from $A_k(t,x)$ to $B_k(t,x)$ or conversely from $B_k(t,x)$ to $A_k(t,x)$. With the expression of the current (34), this small modification of the data induces a jump of the value of the current. Therefore, even if this method does not constraint the time step, Δt should be sufficiently small to have a good accuracy in the calculation of the origins of the characteristics. Furthermore, the more iterations in time we make, the higher the computational time is : we need in fact to recalculate all the trajectories until their origin.

2.5. **Numerical results**

In order to compare the computational time and the relative error of these methods, we consider the case of a constant given electrostatic field E in the Vlasov equation (29). The boundary condition is assumed fully reflective: $\alpha = 1$. Then, we can compute explicitly the exact solution of the Vlasov equation at the equilibrium. The physical numerical values used here are the one of the electrons of the plasma in geostationary orbit, therefore the evolution in time is really fast and the time step Δt should be taken very small.

We consider the space domain $[-L - h_d, -h_d] \cup [h_c, L + h_c]$ that we mesh by N_x nodes $(x_i)_{1\le i\le N_x}$ with a constant step $x_{i+1} - x_i = \Delta x$. The velocity domain is given by $[-2{*}V_{therm}, 2{*}V_{therm}]$ where $V_{therm} = \sqrt{kT_e/m_e}$ is the thermal velocity. We take N_v different values of the velocity in this interval. We assume that a spacecraft is located in $[-h_d, h_c]$ and we chose the numerical values $h_d = 0$, $h_c = 10$, $L = 10000$. The problem is to solve the Vlasov equation (5) coupled with the initial condition (7), the infinite boundary condition (8) and the specular reflection condition (10) with $\alpha = 1$.

In this case, the exact solution for $t \ge 5.10^{-3}$ s (time for which the equilibrium is reached) can be computed exactly and is represented in green in Figure 3. The blue curves represent the computed values of the electron density for $t = 1.25\,10^{-4}$, $2.5\,10^{-4}$, $3.75\,10^{-4}$, $\cdots$. We notice the convergence of the blue curves towards the exact solution. For $t = 5.10^{-3}$ s, the relative error ε_{rr} for the density between the exact solution and the

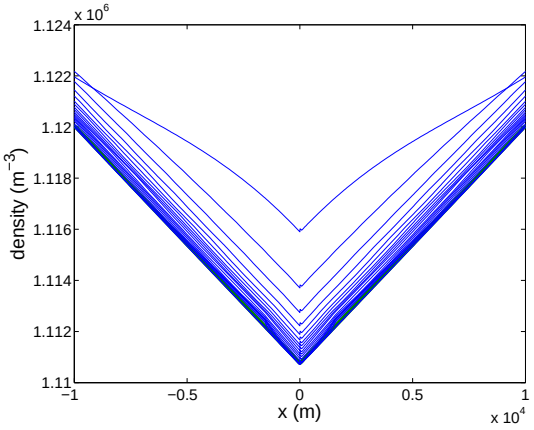

FIGURE 3. Evolution in time of the density of electrons in the geostationary magnetospheric plasma (in blue). The green curve represents the theoretical value of the distribution function at the equilibrium reached for $t \geq 5.10^{-3}$ s.

computed value is estimated, ε_{rr} being defined by

$$\varepsilon_{rr} = \max_{i=1,\ldots,N_x} \frac{|n_{exac}(x_i) - n_{app}(x_i)|}{n_{exac}(x_i)}, \tag{35}$$

where n_{exac} is the exact solution and n_{app} is the approximated solution obtained with our algorithm.

The computational time and the relative errors are reported in Table 1 where we use the abbreviation FV for finite volume method, SL for semi-lagrangian with spline Hermite interpolation method and BackTraj for Back-Trajectory method. Results have been obtained with a 2.66 GHz CPU processor.

TABLE 1. Comparison of the relative error and the computational time between a finite volume method (FV), a semi-lagrangian method (SL) and a Back-Trajectory method (BackTraj) for the resolution of the Vlasov equation.

	CPU Time			Relative error ε_{rr}		
Nb nodes	FV	SL	BackTraj	FV	SL	BackTraj
$N_x = 200$, $N_v = 100$	$1h15'$	$3'51''$	$4h50'$	2.09×10^{-4}	1.73×10^{-4}	2.54×10^{-4}
$N_x = 300$, $N_v = 100$	$2h04'$	$5'41''$		1.96×10^{-4}	1.46×10^{-4}	3.04×10^{-4}
$N_x = N_v = 200$	$4h34'$	$6'43''$		3.53×10^{-4}	2.41×10^{-4}	8.62×10^{-5}
$N_x = 300$, $N_v = 200$	$7h02'$	$15'24''$	$6h27'$	6.22×10^{-5}	2.41×10^{-4}	5.79×10^{-5}
$N_x = 350$, $N_v = 200$		$12'29''$			2.41×10^{-4}	5.03×10^{-5}
$N_x = N_v = 300$		$15'46''$			1.65×10^{-4}	7.21×10^{-5}

- For the finite volume method, the CFL condition imposes a very restrictive bound on the time step: $\Delta t < \Delta x/(2V_{therm}) \simeq 5.10^{-7}$ s ! Furthermore, if we choose $\Delta t = 0.5\,10^{-8}$, the CFL condition is satisfied but oscillations appears in the computed solution (see Figure 4). To avoid this phenomena, we have to take a time step even smaller in order to satisfy largely the CFL condition. In the tests, we have taken $\Delta t = 2.5\,10^{-9}$ s, therefore 2.10^6 iterations are necessary to reach the equilibrium. It implies a long computational time and when $N_x \geq 350$ we have to choose a smaller time step to avoid the phenomenon observed in Figure 4. For this reason the table has not been completed for $N_x \geq 350$. The relative error is good since the method is of second order.

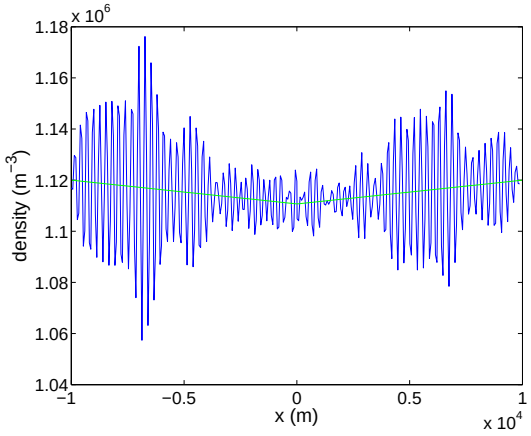

FIGURE 4. Apparition of oscillations for large time with the finite volume method when the time step Δt is close to the upper bound imposed by the CFL condition.

- For the semi-lagrangian (SL) and Back-Trajectory methods, we have taken a time step $\Delta t = 2.5\,10^{-7}$ s. Less iterations are then necessary than for finite volume to reach the equilibrium. Thus the computational time for the semi-lagrangian method is shorter even if we have tridiagonal matrices to inverse (see Appendix). Moreover the high order interpolation method allows us to obtain a good relative error.
- Computational time for the Back-Trajectory method is really long. In fact at each iteration all the trajectories must be recalculated for all the positions of the phase space: the algorithm computes the distribution function at time t^{n+1} without using the one at t^n. Therefore for large time, the method is very time consuming. However, the memory size required is small and we can compute the solution and the relative error at a given time with only one iteration since in that particular case E is constant. Consequently, Table 1 presents only the relative error for most cases. This error is better than the one observed for the others methods. Indeed for E constant, the trajectories are parabolic and easy to compute.

  Despite the long computational time of this last method, we have to keep in mind that this method allows to compute the density and the current only on some nodes x_i of the mesh. Moreover this is the only one which does not impose a constraint on the time step. The following table presents the relative error ε_{rr} computed for different time steps by the Back-Trajectory method. We notice that the relative error remains good even if we take a time step 10 times greater. However, when the time step becomes too large, we can not improve the error even if we take a very thin grid. This remark highlights the numerical noise inherent to particles methods.

	$N_x = 200$, $N_v = 200$	$N_x = 300$, $N_v = 200$	$N_x = 300$, $N_v = 300$	$N_x = 500$, $N_v = 500$
$\Delta t = 2.5 \times 10^{-7}$ s	8.62×10^{-5}	5.79×10^{-5}	7.21×10^{-5}	4.64×10^{-5}
$\Delta t = 2.5 \times 10^{-6}$ s	1.04×10^{-4}	7.96×10^{-5}	7.35×10^{-5}	4.64×10^{-5}
$\Delta t = 2.5 \times 10^{-5}$ s	1.40×10^{-3}	1.39×10^{-3}	1.39×10^{-3}	1.39×10^{-3}

In conclusion, the semi-lagrangian method seems to be the most performing for this problem: good accuracy and low computational time for algorithms with many iterations. The Back-Trajectory method can be promising if the Vlasov equation has to be solved only on some nodes of the mesh and if the accuracy required allows to take a time step not too small. The finite volume method cannot compete due to too severe stability conditions. In a fully 3-dimensional framework the semi-lagrangian method is yet too demanding in term of memory size to be implemented. Therefore the Back-Trajectory method is a good compromise.

3. Numerical results for a 1D model of spacecraft charging

3.1. **Description of the algorithm**

We consider now the whole model presented in Section 1. In the Vlasov equation, the electrostatic potential E is no more constant but derives from a potential solution of the Poisson equation. The main goal is to compute $\phi_{abs}(t)$ and $\Phi'(t,-h_d)$ by solving (21)–(22). To this end, we use an implicit in time scheme for ϕ_{abs} and explicit for Φ'. The main reason for using such a scheme is that if we want to apply it for higher dimensions, we have to keep in mind that the differential potential is not constant on the surface of the spacecraft. The function Φ' in this case is then dependent on the position x and the algorithm is really much more expensive if we do it implicitly. Therefore, knowing the values at $t=t^n$, the scheme writes :

$$J_{ext}\big[\phi_{abs}^{n+1}\Phi_{ref}+(\Phi')^n\big](-h_d)=J_{ext}\big[\phi_{abs}^{n+1}\Phi_{ref}+(\Phi')^n\big](h_c), \tag{36}$$

$$C_d\frac{(\Phi')^{n+1}(-h_d)-(\Phi')^n(-h_d)}{\Delta t}+S_d(\Phi')^n(-h_d)=J_{ext}\big[\phi_{abs}^{n+1}\Phi_{ref}+(\Phi')^n\big](-h_d). \tag{37}$$

In this system, we use the notation

$$\begin{cases} J_{ext}[\phi_{abs}\Phi_{ref}+\Phi'](h_d)=(1-\alpha)\ e\displaystyle\int_{v<0} v(f_i-f_e)\ \mathrm{d}v,\\ J_{ext}[\phi_{abs}\Phi_{ref}+\Phi'](-h_c)=(1-\alpha)\ e\displaystyle\int_{v>0} v(f_i-f_e)\ \mathrm{d}v, \end{cases}$$

to underline the fact that f_i and f_e are (approximations of) solutions of the following Vlasov equation :

$$\partial_t f_{i/e}+v\cdot\partial_x f_{i/e}+\frac{q_{i/e}}{m_{i/e}}(\phi_{abs}\partial_x\Phi_{ref}+\partial_x\Phi')\cdot\partial_v f_{i/e}=0, \tag{38}$$

coupled with boundary conditions (8) and (10).

Equations (36) and (37) correspond to a time discretization of (21) and (22), ϕ_{abs} being treated implicitely, Φ' explicitely. Actually, the treatment of the constraint (36) we propose can be understood by coming back to (18) which can be recast as

$$\begin{aligned}\epsilon_0\partial_t\Big[\phi_{abs}(t)\big(\partial_x\Phi_{ref}(-h_d)-\partial_x\Phi_{ref}(h_c)\big)\Big]+\epsilon_0\partial_t\Big[\partial_x\Phi'(t,-h_d)-\partial_x\Phi'(t,h_c)\Big]\\ =J_{ext}(-h_d)-J_{ext}(h_c)\end{aligned}$$

by using (12). Bearing in mind the asymptotic regime in Section 1.4 and neglecting the time variation of the differential potential Φ', it appears as a stiff ODE determining ϕ_{abs}. Accordingly, let us denote

$$C_{ap}=\partial_x\Phi_{ref}(-h_d)-\partial_x\Phi_{ref}(h_c);$$

then, ϕ_{abs}^{n+1} is defined by the implicit relation

$$\epsilon_0 C_{ap}\ \frac{\phi_{abs}^{n+1}-\phi_{abs}^n}{\Delta t}=J_{ext}\big[\phi_{abs}^{n+1}\Phi_{ref}+(\Phi')^n\big](-h_d)-J_{ext}\big[\phi_{abs}^{n+1}\Phi_{ref}+(\Phi')^n\big](h_c) \tag{39}$$

(where $\epsilon_0 C_{ap}\ll 1$).

Clearly, the reference potential Φ_{ref} defined in (11) should be calculated only once at the beginning of the procedure. Next, knowing $(\Phi')^n(-h_d)$, equation (39) is a nonlinear equation for the unknown ϕ_{abs}^{n+1}. The resolution of this nonlinear equation involves the resolution of the Vlasov equations (38) for f_i and f_e and the decomposition of Φ with ϕ_{abs} and Φ' does not allows to solve immediately the Poisson equation in this step.

Once we have obtained ϕ_{abs}^{n+1}, we can first solve equation (37) for the unknown $(\Phi')^{n+1}(-h_d)$, and, next, the last step consists in solving the Poisson equation (13) to update the differential potential Φ' in the whole domain. The algorithm is then composed of the following steps :

(1) Initialization : we compute the reference potential Φ_{ref} and initialize the value of the distribution functions.
(2) Resolution of the nonlinear equation (39) : since the derivative of J_{ext} with respect to ϕ_{abs} is difficult to compute, we use in this step a quasi-Newton method. An advantage of this method is that no constraint on the time step is needed to guarantee the convergence of the scheme. In fact in this case the right hand side of (39) is a decreasing function with respect to ϕ_{abs}^{n+1}, since it has been observed that the spacecraft receives less current from the magnetosphere when the potential on the conductor body increases. The rigorous mathematical proof of this result is still a work in progress. A loop for the computation of ϕ_{abs}^{n+1} is implemented involving several resolutions of the Vlasov equation. The three methods presented in the previous section are used for the calculation of J_{ext}. We notice that in this step we only need to calculate J_{ext} at the two nodes $x = -h_d$ and $x = h_c$.
(3) Computation of $(\Phi')^{n+1}(-h_d)$ thanks to (37).
(4) Resolution of the Poisson equation (13) with the boundary condition for $x = -h_d$ obtained in step 3. We use $\mathbb{P}1$ finite element approximation (which in the present one dimension framework coincides with the standard finite difference approximation). The computation of the densities n_i and n_e in the whole computational domain is necessary.
(5) Go back to the second step for the next iteration in time.

In this description, the second step is the most demanding in terms of computational time since we need several resolutions of the Vlasov equation to solve the nonlinear equation (39). On the contrary, for a given time step, we solve only one Poisson equation in step 4. No constraint on the time step is necessary for the convergence of this algorithm. For these reasons, the resolution of the Vlasov equation is the more challenging issue in the whole computational strategy.

3.2. **Numerical simulations**

A numerical simulation of the charging of a 1D spacecraft is obtained thanks to the algorithm presented above. The numerical values used are the one of the plasma in geostationary orbit. The three methods of resolution of the Vlasov equation are implemented. The evolution with respect to time of the absolute potential ϕ_{abs} and of the differential potential $\Phi'(-h_d)$ are given in Figure 3.2 for several values of the reflection parameter: $\alpha = 0$, $\alpha = 1/3$, $\alpha = 2/3$, respectively. In case of total reflection $\alpha = 1$, as already remarked, the spacecraft does not receive any flux from its environment: we have then $\phi_{abs} = \Phi' = 0$ for all time. In this simulation, we have chosen $N_x = 500$ nodes and $N_v = 200$ nodes. For each method, we run the algorithm until we reach the final time $T_f = 1.5\,10^{-4}$ s. at which the unknowns have reach stabilized states.

Since the current of electrons is initially much larger than the current of ions, the spacecraft charges negatively. Then, it acts repulsively on electrons and attractively on ions so that a stationary state can be exhibited, with a differential potential which remains small compared to the absolute potential. All these features can be observed on real simulations, despite the simplicity of our toy-model. The simulations reveal a behavior highly sensitive to the value of α. As α decreases, the charge increases faster in the earlier times, and it reaches higher limit value. It corresponds to the physical intuition since for $\alpha = 0$ all incoming particles are caught by the boundary. Changing the value of α can be compared with the situation where the spacecraft passes from darkness ($\alpha = 0$) to light where photoemission phenomena should be accounted for ($\alpha > 0$). All these phenomena are interesting and certainly deserve further mathematical analysis, with all the necessary criticism to extend practical information due to the oversimplified geometry. Let us comment further on the performances of the numerical methods.

The first observation is that the discrepancies between the three methods remain very small, at least in the considered time interval. The time step is taken in order to respect the constraint imposed by the finite volume method and by the semi-lagrangian method. Table 2 reports the CPU time required with a processor 2.66 GHz

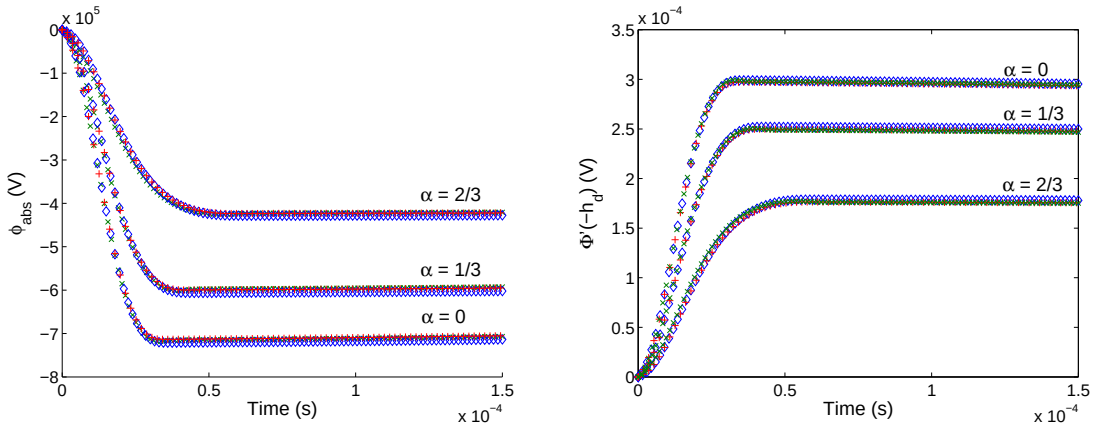

FIGURE 5. Absolute potential (left) and differential potential (right) with respect to the time for the finite volume (green cross), semi-lagrangian (red plus sign) and Back-Trajectory (blue diamond) methods and for several value of the reflection parameter α.

TABLE 2. Comparison of CPU time for each method

Method	Time step Δt (nb of iterations)	Nb of nodes (N_x, N_v)	Relative error	CPU time
VF	$\Delta t = 3.\,10^{-9}$ s (50000 it)	$(500, 200)$	0.16	$1h10'$
SL	$\Delta t = 1.5\,10^{-8}$ s (10000 it)	$(500, 200)$	0.03	$46'08''$
SL	$\Delta t = 3.\,10^{-8}$ s (5000 it)	$(500, 200)$	0.03	$18'01''$
BackTraj	$\Delta t = 3.\,10^{-8}$ s (5000 it)	$(500, 200)$	0.1	$27h35'$
BackTraj	$\Delta t = 1.5\,10^{-7}$ s (1000 it)	$(500, 200)$	0.12	$1h07'$
BackTraj	$\Delta t = 3.\,10^{-7}$ s (500 it)	$(500, 200)$	0.13	$17'30''$

and the relative error obtained. This error is defined with formula (35) where n_{exac} is computed with 5000 nodes for the semi-lagrangian method, (actually in this case, the relative errors between the three methods for 5000 nodes is lesser than 1%).

We first remark that the relative error is better with the semi-lagrangian method. Concerning the computational time, the previous conclusions are still available. However, an important point has to be underlined. As precised above, the second step of the algorithm needs the computation of J_{ext} only on the two nodes $x = -h_d$ and $x = h_c$. The Back-Trajectory method allows to compute the distribution function only on these particular points of the mesh. Therefore the computation of ϕ_{abs} is settled fastly with this method. The resolution of the Vlasov equation in the whole computational domain is then implemented only to compute the densities in step 4. Actually if we compute by this method the distribution function everywhere for each iteration of step 2, CPU time is more than 5 times greater : calculation takes 6h for 1000 iterations and 2h for 500 iterations. Moreover, the Back-Trajectory method is less constrained by stability condition and we can choose a larger time step to run the simulation faster. Nevertheless the results become less accurate and the numerical noise inherent to this method can bother the convergence of loop in step 2. For instance for $\Delta t = 5.\,10^{-7}$ s the algorithm does not converge for the calculation of ϕ_{abs}. Since the algorithm recalculates all trajectories from their origin for each iteration, the CPU time is very high when the number of iterations becomes large, i.e. when we want to study long time behavior of the solution.

4. Conclusion

(1) In simple geometries, the semi-lagrangian method seems to be the most promising. However, the memory capacities needed prevent applying this method in 3D. Finite volume schemes are penalized by stability conditions, at least with the physical parameters considered here. On the contrary the Back-Trajectory method needs less memory capacity and it provides accurate enough results.
(2) To increase the code speed, a parallelization of the Vlasov solver can be considered. Since each trajectory is self-supported, PIC methods can be easily parallelized by computing characteristics on different processors. For the semi-lagrangian and the finite volume methods, the parallelization needs more effort. In fact splitting the computational space into several domains, these domains are not independent one from each other. If we treat them separately on different processors, we have to take care of interface conditions. A parallelization procedure of the semi-lagrangian method is presented in [13].
(3) The Back-Trajectory method becomes particularly interesting when we use the geostationary approximation. In such a case the Poisson equation is simplified into the Laplace equation, see (4). Therefore, we do not need in step 4 to compute the densities n_i and n_e. It implies that in the algorithm the Vlasov equation is solved only to calculate J_{ext} on the boundary nodes. The Back-Trajectory method is the one which allows us to compute these values of J_{ext} without solving the Vlasov equation in the whole computational domain. In turn the CPU time gain is particularly significant while the boundary currents are naturally evaluated with accuracy. Furthermore, parallelization appears in a quite natural way and does not require a huge and intricate development work. For these reasons, the Back-Trajectory method is well-suited for the simulation of spacecraft charging in GEO atmospheres. The software SPARCS uses this method, and the current version already includes paralellized procedures with a close to the optimal speed-up. As far as there is no geometry simplification, this is the most efficient approach and further developments of the code will incorporate more involved physics (multi reference potentials, reflection laws,...). It can also be adapted to different situations, where volume charges are accounted for and the present study shows that it still keeps its main advantages.

Appendix A. Boundary conditions for the semi-lagrangian method

The spline Hermite interpolation used for the semi-lagrangian method has proved its efficiency for obtaining accurate solutions of the Vlasov equation (see [17, 29]). We recall shortly the main idea of this high order interpolation method.

Letting $(x_i)_{i=0,\cdots,N}$ being $N+1$ nodes such that $x_i = x_0 + i\cdot h$ where h is the mesh size : $h = (x_N - x_0)/(N+1)$. The projection s of f onto the cubic spline basis reads :

$$f(x) \simeq s(x) = \sum_{\nu=-1}^{N+1} \eta_\nu B_\nu(x),$$

where B_ν is the cubic B-spline

$$B_\nu(x) = \frac{1}{6h^3} \begin{cases} (x - x_{\nu-2})^3 & x \in [x_{\nu-2}, x_{\nu-1}], \\ h^3 + 3h^2(x - x_{\nu-1}) + 3h(x - x_{\nu-1})^2 - 3(x - x_{\nu-1})^3 & x \in [x_{\nu-1}, x_\nu], \\ h^3 + 3h^2(x_{\nu+1} - x) + 3h(x_{\nu+1} - x)^2 - 3(x_{\nu+1} - x)^3 & x \in [x_\nu, x_{\nu+1}], \\ (x_{\nu+2} - x)^3 & x \in [x_{\nu+1}, x_{\nu+2}], \\ 0 & \text{otherwise.} \end{cases}$$

The interpolating spline s is uniquely determined by the $(N+1)$ conditions

$$f(x_i) = s(x_i), \qquad \forall\, i = 0, \cdots, N,$$

with the Hermite boundary conditions at the ends of the interval which allows to construct a C^1 global approximation :

$$f'(x_0) \simeq s'(x_0), \qquad f'(x_N) \simeq s'(x_N).$$

The only cubic B-spline not vanishing at point x_i are $B_{i\pm1}(x_i) = 1/6$ and $B_i(x_i) = 2/3$. Then the interpolating conditions lead to

$$f(x_i) = \frac{1}{6}\eta_{i-1} + \frac{2}{3}\eta_i + \frac{1}{6}\eta_{i+1}, \quad i = 0, \cdots, N.$$

Moreover, we have $B'_{i\pm1}(x_i) = \pm 1/(2h)$ and $B'(x_i) = 0$. Thus the Hermite boundary conditions imply

$$\begin{aligned} f'(x_0) \simeq s'(x_0) &= -\frac{1}{2h}\eta_{-1} + \frac{1}{2h}\eta_1, \\ f'(x_N) \simeq s'(x_N) &= -\frac{1}{2h}\eta_{N-1} + \frac{1}{2h}\eta_{N+1}. \end{aligned}$$

Finally, the computation of $(\eta_{-1}, \cdots, \eta_{N+1})$ involves the inversion of a $(N+3) \times (N+3)$ matrix. In our algorithm, the inverse of this matrix is determined thanks to a LU decomposition.

In order to obtain an accurate interpolation, we have to use a high order approximation of the derivatives at x_0 and x_N. The originality of this problem is due to the fact that we use specular boundary conditions in the end point of the domain representing the spacecraft and infinite boundary conditions in the external boundary of the interval : for instance, we assume that $[x_0, x_N]$ is the interval $[-L - h_c, -h_c]$, therefore

$$\begin{aligned} f(x_0, v) &= f_\infty(v), && \text{for } v > 0, \\ f(x_N, v) &= f(x_N, -v), && \text{for } v < 0. \end{aligned}$$

Contrary to the case of periodic boundary conditions (see [13]), the values of the function outside $[x_0, x_N]$ can not be known. Therefore we have to use the values of f at time t^n inside this interval to compute the distribution function at time $t^n + \Delta t$. Thanks to our boundary conditions, at the boundary we only have to compute $f(t^n + \Delta t, x_0, v)$ for $v < 0$ and $f(t^n + \Delta t, x_N, v)$ for $v > 0$. This can be easily done with the procedure described in section 3.3 since for $v < 0$, $X(t^n; x_0, v, t^{n+1}) \in [x_0, x_N]$ and for $v > 0$, $X(t^n; x_N, v, t^{n+1}) \in [x_0, x_N]$. Moreover to obtain an accurate approximation of the derivatives, we use the Taylor identities :

$$\begin{cases} f(x+h) = f(x) + hf'(x) + \dfrac{h^2}{2}f''(x) + \dfrac{h^3}{6}f^{(3)}(x) + \dfrac{h^4}{24}f^{(4)}(x) + o(h^4). \\ f(x+2h) = f(x) + 2hf'(x) + 2h^2f''(x) + \dfrac{4h^3}{3}f^{(3)}(x) + \dfrac{2h^4}{4}f^{(4)}(x) + o(h^4). \\ f(x+3h) = f(x) + 3hf'(x) + \dfrac{9h^2}{2}f''(x) + \dfrac{9h^3}{2}f^{(3)}(x) + \dfrac{27h^4}{8}f^{(4)}(x) + o(h^4). \end{cases}$$

Thus we deduce that

$$f(x+3h) - \frac{9}{2}f(x+2h) + 9f(x+h) - \frac{11}{2}f(x) = 3hf'(x) + \frac{3}{4}h^4f^{(4)}(x) + o(h^4).$$

Then we find the following approximation for the derivative in x_0 :

$$f'(x_0) = \frac{1}{3h}(f(x_3) - \frac{9}{2}f(x_2) + 9f(x_1) - \frac{11}{2}f(x_0)). \tag{40}$$

And by the same token, we obtain :

$$f'(x_N) = -\frac{1}{3h}(f(x_{N-3}) - \frac{9}{2}f(x_{N-2}) + 9f(x_{N-1}) - \frac{11}{2}f(x_N)). \tag{41}$$

This idea is similar to the one used in WENO-type interpolations methods (see [8] and references therein) for reconstruction of smooth solutions.

References

[1] R. Belaouar, N. Crouseilles, P. Degond, E. Sonnendrücker, *An asymptotically stable semi-lagrangian scheme in the quasi-neutral limit*, preprint (2007).

[2] C. K. Birdsall, A. B. Langdon, *Plasma Physics via Computer Simulation*, Institute of Physics Publishing, Bristol and Philadelphia, 1991.

[3] M. Cho, *Arcing on high voltage solar arrays in low earth orbit: theory and computer particle simulation*, Ph.D. thesis, Massachusetts Institute of Technology, February 1992.

[4] J.-P. Chehab, A. Cohen, D. Jennequin, J. J. Nieto, Ch. Roland, J.-R. Roche, *An adaptive particle-in-cell method using multiresolution analysis*, in Numerical methods for hyperbolic and kinetic problems, IRMA Lect. Math. Theor. Phys., vol. 7, S. Cordier, T. Goudon, M. Gutnic and E. Sonnendrücker Eds. (Eur. Math. Soc., Zürich, 2005) pp. 29–42.

[5] G.-H. Cottet, P.-A. Raviart, *Particle methods for the one-dimensional Vlasov–Poisson equations*, SIAM J. Numer. Anal. **21** 1 (1984) 52–76.

[6] P. Crispel, *Modélisation mathématique et simulation de la transition d'une décharge électrostatique primaire vers un arc électrique secondaire entretenu par la puissance photovoltaïque d'un générateur solaire de satellite*, PhD thesis, Université Paul Sabatier Toulouse III, 2006.

[7] P. Crispel, P. Degond, M.-H. Vignal, *Quasi-neutral fluid models for current-carrying plasmas*, J. Comput. Phys., **205** 2 (2005) 408–438.

[8] J. A. Carrillo, F. Vecil, *Non-oscillatory interpolation methods applied to Vlasov-Based models*, SIAM J. Sci. Comput. **29** 3 (2007) 1179–1206.

[9] O. Chanrion, *Simulation de l'influence de la propulsion plasmique sur la charge électrostatique d'un satellite en milieu magnétosphérique*, PhD Thesis, Ecole Nationale des Ponts et Chaussées, 2001.

[10] M. Chane-Yook, S. Clerc, S. Piperno, *Space charge and potential distribution around a spacecraft in a isotropic plasma*, J. Geophys. Res. - Space Physics **111** (2006).

[11] S. Clerc, S. Brosse, M. Chane-Yook, *Sparcs : an advanced software for spacecraft charging analysis*, 8th Spacecraft Charging Tech. Conf., Huntsville, Alabama, 2003.

[12] N. Crouseilles, F. Filbet, *Numerical approximation of collisional plasma by high order methods*, J. Comp. Phys. **201**, 2 (2004) 546–572.

[13] N. Crouseilles, G. Latu, E. Sonnendrücker, *Hermite spline interpolation on patches for parallely solving the Vlasov-Poisson equation*, Int. J. Appl. Math. Comput. Sc. **17**, 3 (2007) 101–115.

[14] P. Degond, F. Deluzet, L. Navoret, *An asymptotically stable Particle-In-Cell (PIC) scheme for collisionless plasma simulations near quasineutrality*, C. R. Acad. Sci. Paris, Ser. I **343** (2006) 613–618.

[15] V. Grandgirard, M. Brunetti, P. Bertrand, N. Besse, X. Garbet, P. Ghendrih, G. Manfredi, Y. Sarazin, O. Sauter, E. Sonnendrücker, J. Vaclavik, L. Villard, *A drift-kinetic semi-Lagrangian 4D code for ion turbulence simulation*, J. Comput. Phys. **217** (2006) 395–423.

[16] J. Forest, A. Hilgers, B. Thiebault, L. Eliasson, J.-J. Berthelier, H. de Feraudy, *An open-source spacecraft plasma interaction simulation code PicUp3D: tests and validations* , IEEE Trans. Plasma Sc. **34** (2006) 2103–2113.

[17] F. Filbet, E. Sonnendrücker, P. Bertrand, *Conservative numerical schemes for the Vlasov equation*, J. Comput. Phys. **172** (2001) 166–187.

[18] F. Filbet, E. Sonnendrücker, *Comparison of Eulerian Solver*, Comput. Phys. Commun. **150** (2003) 247–266.

[19] A. Ghizzo, P. Bertrand, M. Shoucri, T.W. Johnston, E. Filjakow, M.R. Feix, *A Vlasov code for the numerical simulation of stimulated Raman scattering*, J. Comput. Phys. **90** (1990) 431.

[20] R. J. LeVeque, *Numerical Methods for Conservation Laws*, Lectures in Mathematics, ETH-Zurich (Birkhauser-Verlag, Basel, 1990).

[21] L. Lévy, *Charge des matériaux et systèmes en environnment spatial*, CERT–ONERA, in Space environment prevention of risks related to spacecraft charging, ed. Cepaduès-éditions, Toulouse, F, 1996.

[22] M. J. Mandell, V. A. Davies, L. G. Mikelides, *NASCAP-2K Preliminary Documentation*, Science Applications International Corp, San Diego, CA, Scientific rept. no. 2, A555024, 2002.

[23] M. J. Mandell, V. A. Davies, D. L. Cooke, A. T. Wheelock, C. J. Roth, *Nascap-2k spacecraft charging code overview*, IEEE Trans. Plasma Sc. **34** (2006) 2084–2093.

[24] A. P. Plokhikh, V. G. Malko, V. A. Semenov, *Escape software modeling for the electrostatic charging with electric propulsion in the ionosphere earth*, Manuel d'utilisation v-1, Research Institute of Applied Mechanics and Electrodynamics, Moscou, 1998.

[25] J.-F. Roussel, *Spacecraft plasma environment and contamination simulation code: description and first tests*, Journal of Spacecraft and Rockets **35** (1998) 205–211.

[26] J.-F. Roussel, *Modelling of spacecraft plasma environment interactions*, in Spacecraft Charging Technology, Proceedings of the Seventh International Conference held 23-27 April, 2001 at ESTEC, Noordwijk, the Netherlands. Edited by R.A. Harris, European Space Agency, ESA SP-476, 2001.

[27] J. F. Roussel, F. Rogier, M. Lemoine, D. Volpert, G. Rousseau, G. Sookahet, P. Sng, A. Hilgers, *Design of a new modular spacecraft plasma interaction modeling software (SPIS)*, Proceedings of the 8th Spacecraft Charging Tech. Conf., Huntsville, AL, October 20-24, 2003.

[28] M. Shoucri, G. Knorr, *Numerical integration of the Vlasov equation*, J. Comput. Phys. **14** (1974) 84–92.

[29] E. Sonnendrücker, J. Roche, P. Bertrand, A. Ghizzo, *The semi-lagrangian method for the numerical resolution of the Vlasov equation*, J. Comput. Phys. **149** (1999) 201–220.

[30] E. Sonnendrücker, *Méthodes semi-Lagrangiennes pour la résolution numérique de léquation de Vlasov*, Lecture notes CEA-EDF-INRIA School on "Modèles numériques pour la fusion contrôlée, Nice, Sept. 2008.